Multiparametric ultrasound and machine learning for prostate cancer localization

Chen, Peiran; Calis, Metin; Wijkstra, Hessel; Huang, Pintong; Hunyadi, Borbála; Mischi, Massimo

Important note
To cite this publication, please use the final published version (if applicable).
Please check the document version above.

Multiparametric ultrasound and machine learning for prostate cancer localization

Peiran Chen[1], Metin Calis[2], Hessel Wijkstra[1,3], Pintong Huang[4], Borbála Hunyadi[2], Massimo Mischi[1]

[1] Dept. Electrical Engineering, Eindhoven University of Technology, Eindhoven, Netherlands
[2] Dept. Microelectronics, Technical University of Delft, Delft, Netherlands
[3] Dept. Urology, Amsterdam University Medical Centers, Amsterdam, Netherlands
[4] Dept. Ultrasound in Medicine, The Second Affiliated Hospital of Zhejiang University, Hangzhou, China

Abstract—A cost-effective, widely available, and practical diagnostic imaging tool for prostate cancer (PCa) localization is still lacking. Recently, the contrast-ultrasound dispersion imaging (CUDI) technique has been developed for PCa localization by quantifying dynamic contrast-enhanced ultrasound (DCE-US) acquisitions. Tissue stiffness is an additional PCa biomarker that can be quantified by ultrasound shear-wave elastography (SWE). In this work, a dedicated preprocessing of 3D DCE-US acquisitions was investigated by using multilinear singular value decomposition (MLSVD), aiming at improving the CUDI performance. Moreover, the diagnostic potential of a multiparametric ultrasound imaging approach combining 3D CUDI features with SWE tissue elasticity for clinically significant (cs)PCa localization was evaluated by comparison with the histopathological outcome of systematic biopsies. In this multiparametric approach, the performance of five classifiers was evaluated and compared for biopsy-region csPCa classification. The classification performance was assessed by the area under the Receiver Operating Characteristics curve (AUC) in a k-fold cross validation fashion comprising sequential floating forward selection of the features. The combination of CUDI features with MLSVD preprocessing and SWE elasticity yielded the best AUC=0.87 for csPCa localization. Our results suggest 3D multiparametric ultrasound imaging approach combing a dedicated preprocessing step to be a useful tool for PCa diagnostics.

Index Terms—ultrasound, prostate cancer, machine learning, multilinear singular value decomposition

I. INTRODUCTION

Prostate cancer (PCa) is the second leading cause of cancer mortality in men in western countries [1]. In clinical routine, the 12-core systematic biopsy (SBx) procedure guided by transrectal ultrasound work as the gold standard for PCa diagnosis. However, biopsies suffer from a risk of infection, the underdiagnosis of significant PCa, and overtreatment of insignificant cancer [2], [3]. Improving the diagnostic efficacy of SBx or even replacing SBx with non-invasive imaging diagnostics tools is in demand. Multiparametric magnetic resonance imaging (MRI) has been established as a valuable imaging tool for the detection of significant PCa [4]. However, poor reproducibility and specificity, along with the high cost and limited availability of multiparametric MRI, evidence the need for cost-effective, widespread imaging alternatives that especially capable of localizing clinically significant (cs)PCa, so as to enable timely treatment of aggressive tumors.

Recently, dynamic contrast-enhanced ultrasound (DCE-US) has been considered as one of the candidates for PCa diagnosis; especially 3D DCE-US enables the visualization and analysis of the entire prostate gland. Tumor-driven angiogenesis is a recognized indicator of PCa, resulting in a complex and irregular microvascular architecture [5]. Tumor perfusion patterns become thus distinguishable from those in normal tissue, establishing the basis for the diagnosis of cancer by the analysis of the blood flow patterns [6]. DCE-US provides the real-time visualization of the blood flow with the help of intravenously-injected ultrasound contrast agents (UCAs), which can highlight those changes in the microvascular network associated with cancer angiogenesis. The temporal evolution of the UCA local concentrations is reflected in pixel intensity variations over the DCE-US loops. Time-intensity curves (TICs) can be measured at each pixel by collecting these variations.

In the past years, our previous work has shown the value of convective-dispersion modeling for interpreting the measured TICs. Based on that, several contrast-ultrasound dispersion imaging (CUDI) techniques have been developed to quantitatively analyze the DCE-US acquisitions by the extraction of perfusion and dispersion features, obtaining promising results for the localization of PCa [7]–[11].

The DCE-US recordings suffer from multiplicative and additive noise originating from speckle and the UCA transport statistics that hinders the quality of the extracted DCE-US features [12], [13]. In [14], blind source separation of the signal and the noise subspaces has been proposed as a denoising technique. Singular value decomposition (SVD) is shown to outperform the other techniques. The SVD is applied on the flattened four dimensional DCE-US recording where the rows hold the spatial information and the columns represent the temporal information. Due to the flattening process, the information regarding the voxel locations is lost. In [15], multilinear singular value decomposition (MLSVD) is proposed as an extension that generalizes the concept of SVD to multiple dimensions. The volumetric information that is retained by considering the tensor format of the recording is expected to improve the classification performance of the TIC dispersion modeling. Therefore, in this paper we have applied MLSVD preprocessing to all the CUDI features and assessed

its contribution to improved classification.

In addition to vascularity, tissue stiffness is another biomarker of PCa. In the prostate, tissue in tumor regions is generally stiffer than normal tissue due to the changes in cell density and collagen deposition in the tumor regions [16]. Ultrasound shear-wave elastography (SWE) offers a quantitative way to characterize tissue stiffness, providing valuable information to discriminate between benign and malignant prostate tissue [17]. Currently, transrectal SWE is still limited to 2D acquisitions. In this work, we overcome this limitation by performing multi-plane 2D acquisitions on the same prostate with subsequent 3D reconstruction based on the method proposed by Schalk et al. [18].

Finally, in this work we investigate the diagnostic potential of a multiparametric ultrasound imaging approach, enhanced by MLSVD preprocessing, which combines 3D CUDI quantitative features with SWE tissue elasticity for the localization of PCa. For the 3D prostates, a machine learning algorithm was developed for biopsy-region csPCa classification, using the corresponding histopathological findings of SBx as the reference. Five different classifiers were implemented and evaluated. For each classifier, a sequential floating forward selection of the features as well as Bayesian-optimization-based hyperparameter tuning were implemented. The performance of the classifiers for csPCa classification was eventually evaluated and compared based on cross validation results. Hence, the novelty that we bring is three-fold: implementing the dedicated preprocessing method, MLSVD, to improve the classification performance using the CUDI features; demonstrating the added diagnostic value of SWE tissue elasticity to a multiparametric ultrasound imaging approach for PCa localization; and implementing different classifiers together with advanced feature selection and hyperparameter tuning.

II. METHODS

Figure 1 presents the whole processing pipeline of the biopsy-region multiparametric ultrasound imaging for PCa localization, the details of which are elaborated in following sections.

A. Data acquisition

In this study, after signing informed consent, multi-plane 2D SWE acquisitions with manual sweeping from base to apex of the prostate were firstly performed on 54 patients using an Aixplorer scanner (SuperSonic Imagine, France) equipped with a SE12-3 endocavity probe. Subsequently, 3D DCE-US recordings using a LOGIQ E9 scanner (GE HealthCare, USA) equipped with a RIC9-5 transrectal probe were carried out on the same patients following the intravenous administration of a 2.4-mL bolus of SonoVue® (Bracco, Italy). After ultrasound scanning, all the patients underwent a 12-core SBx procedure. The SBx cores were then histopathologically classified as either benign, insignificantly malignant with Gleason 3+3=6, or significantly malignant tissue samples (csPCa). These steps were conducted at the Second Affiliated Hospital of Zhejiang University (China) by an experienced ultrasound examiner and pathologist, respectively.

B. Preprocessing and denosing

Similar to [19], the data is converted from spherical to cartesian with a voxel size of 0.25 mm, and the spatial resolution is equalized to 0.8 mm. The data is then downsampled to a voxel spacing of 0.75 mm, and cropped according to the prostate boundaries which were delineated by two urologists in consensus. Following the method proposed in [15], the DCE-US tensor is unfolded in each mode, SVD is applied and truncated according to the estimated ranks. By considering the multidimensional nature of the DCE-US recording, we expect MLSVD to be a better approach to highlight the bubble kinetics and hence, improve the classification performance of all of the CUDI features.

C. CUDI analysis

The 3D DCE-US acquisitions were quantitatively analyzed by the developed CUDI techniques. The mono-dimensional convective-dispersion equation given in (1) can be employed to model the UCA transport through the prostate as a convective-dispersion process:

$$\partial_t C(z,t) = D\partial_z^2 C(z,t) - v\partial_z C(z,t),\qquad(1)$$

where $C(z,t)$ is the UCA concentration at position z and time t, D is the dispersion coefficient, and v is the convective velocity. In (1), D and v are assumed to be locally constant.

In the **model fit analysis**, an analytical solution of the convective-dispersion equation in (1) is fitted to the measured TICs at each voxel through a mean squared error minimization procedure [7]. The adopted solution of (1) yields the modified local density random walk model [7], which is given as

$$C(t) = \alpha\sqrt{\frac{\kappa}{2\pi(t-t_0)}}\exp\left(-\frac{\kappa(t-t_0-\mu)^2}{2(t-t_0)}\right),\qquad(2)$$

where the scale factor α, representing the time integral of $C(t)$, is related to the UCA dose and the blood flow (mass conservation law), the mean transit time μ represents the average time that the UCA bolus takes to travel from the injection to the detection site, t_0 represents the bolus injection time, and κ is a parameter related to local bolus dispersion. Moreover, typical **perfusion features** such as wash-in time, wash-in rate, peak time, appearance time, and the area under the TIC are also extracted from the fitted TICs [20]–[23].

The multipath trajectories of UCAs through a microvascular network determine the UCA dispersion kinetics, which reflects the underlying microvascular architecture. As the shape similarity between TICs is influenced by the local degree of dispersion, **spatiotemporal similarity analysis** is employed to quantify the similarity between neighboring TICs in a shell-shaped kernel by assessing their spectral coherence, the temporal similarity, and the mutual information [8], [9], [24], [25].

By **system identification**, rather than assessing the similarity between neighboring TICs, these are considered as input
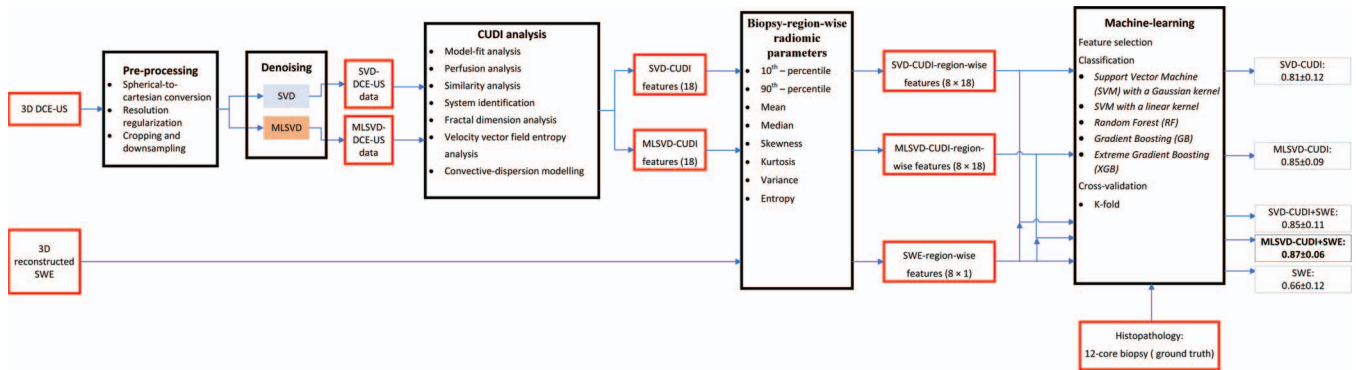
908

Fig. 1. The processing pipeline of the proposed biopsy-region multiparametric ultrasound imaging for PCa localization.

and output of a dilution system, which is then characterized by the identification of its Green's function, which solves (1) for a spatiotemporal Dirac impulse input [10]. The convective (velocity) and dispersion (dispersion coefficient) terms are then estimated separately [10]. These can also be obtained by solving the full **convective-dispersion** equation in a 3D kernel, with the boundary conditions being fully determined by the outer TICs [11]. Based on the obtained convective vector fields, **entropy and conditional entropy of the vector field** are calculated to infer vascular heterogeneity [26]. In addition, **fractal dimension analysis** provides a geometrical measure of the vascular architecture based on the relation between the fractal dimension and relative dispersion in the derived flow map (TIC peak intensity) at multiple scales [27].

Based on the aforementioned CUDI analysis, 18 CUDI features were extracted.

D. 3D SWE

In the prostate, malignant tissue is generally stiffer than benign tissue due to the changes in cell density and collagen deposition in the tumor regions [16]. Ultrasound shear-wave elastography (SWE) offers a quantitative way to characterize the tissue stiffness, enabling us to discriminate between benign and malignant prostate tissue [17]. Therefore, SWE-based elasticity estimates can be considered as a complementary parameter in addition to the CUDI features, supporting the PCa classification process with both vascular and mechanical characterization of tissue.

Recently, 3D transrectal DCE-US recordings have become available, enabling the analysis of the entire prostate. However, transrectal SWE is still limited to 2D acquisitions, which hampers the implementation of 3D multiparametric ultrasound. Therefore, multi-plane 2D acquisitions on the same prostate and subsequent 3D reconstruction was implemented to overcome this limitation. The 3D map of SWE tissue elasticity was reconstructed based on multi-plane 2D SWE acquisitions by assuming regular sampling of the planes at equal-angle intervals from the base to the apex of the prostate. With the obtained angles, the 3D coordinates of each SWE plane were calculated and the elasticity values in 2D planes were assigned to their corresponding positions in the 3D space. Interpolation

of the elasticity values between planes was then implemented by using the nearest neighbor method [18].

E. Biopsy-region-wise radiomic parameters

In this work, all the patients underwent a 12-core SBx procedure. The SBx histopathology results serve as the ground truth, indicating the presence of benign and malignant prostate tissues in the biopsy regions. To achieve the biopsy-region multiparametric ultrasound imaging, the 3D parametric maps resulting from the 3D CUDI analysis and the reconstructed 3D SWE were delineated and then subdivided into 12 regions corresponding to the SBx locations [19]. Moreover, in each region, the median, 10th-percentile, 90th-percentile, mean, skewness, kurtosis, variance, and entropy of each extracted feature were calculated as region-wise radiomic parameters [28]. Therefore, for each prostate, the feature matrix was in the form of 12 (SBx regions) $\times$ 8 (radiomic parameters) $\times$ 19 (18 CUDI features and SWE elasticity).

F. Machine-learning-based multiparametric approach

A machine learning algorithm that processes the region-wise radiomic parameters ($12 \times 8 \times 19$) was implemented to achieve a biopsy-region PCa prediction. In this algorithm, five classifiers, namely Support Vector Machine (SVM) with a Gaussian kernel, SVM with a linear kernel, Random Forest (RF), Gradient Boosting (GB) and extreme Gradient Boosting (XGB), and their respective hyperparameters were firstly evaluated by grid search method, aiming at providing the preliminary optimal hyperparameters. Given the classifiers and their hyperparameters, feature selection was performed using a sequential floating forward selection (SFFS), which was cross-validated in a k-fold fashion [29]. Here, the 54 datasets were divided into 9 folds, in one of which the region-wise radiomic parameters of 6 datasets were used as the observations while the region-wise radiomic parameters of the datasets in the remaining 8 folds were used as the training set. The feature selection procedure gave the best subset of radiomic parameters for each classifier. Subsequently, Bayesian optimization was applied to these classifiers together with the selected feature subsets for tuning the hyperparameters again with the k-fold cross-validation method at the biopsy-region level, from which

TABLE I

CLASSIFICATION PERFORMANCE OF DIFFERENT MULTIPARAMETRIC APPROACH: CUDI ANALYSIS ONLY, SWE ALONE, THE COMBINATION OF CUDI AND SWE, AS WELL AS USING MLSVD PRIOR TO CUDI ANALYSIS.

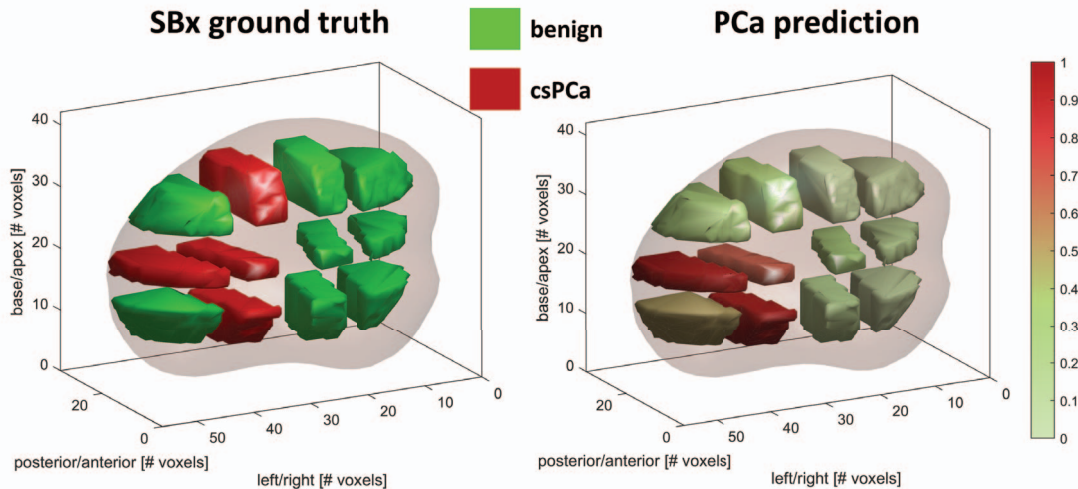|	SVD-CUDI	SWE	SVD-CUDI + SWE	MLSVD-CUDI	MLSVD-CUDI + SWE
AUC (mean ± std) over the folds	0.81 ± 0.12	0.66 ± 0.12	0.85 ± 0.11	0.85 ± 0.09	0.87 ± 0.06

Fig. 2. Example of the histopathologically examined SBx results and the PCa prediction results obtained by the proposed biopsy-region multiparametric ultrasound imaging approach for the 12 subdivided regions in a same prostate.

the classifier having the best PCa classification performance was determined [30]. The area under the Receiver Operating Characteristics curve (AUC) was calculated to evaluate the classification performance. In the cross-validation procedure, the mean and standard deviation (std) of the AUC over the folds were calculated.

III. RESULTS

Of the 54 patients, 20 were found with csPCa based on the SBx histopathology results. Table I compares the biopsy-region multiparametric approach using only the radiomic parameters extracted from CUDI analysis, using the SWE elasticity alone, as well as using the combination of CUDI and SWE elasticity. Moreover, the results obtained by implementing the MLSVD prior to performing CUDI analysis are also used for comparison. Compared to the combination of CUDI and SWE, using only the vascularity-related features (CUDI) or the tissue-stiffness feature (SWE) had lower mean AUC value and larger std, especially that using the SWE alone had AUC of 0.66, which reveals the importance and advantage of the combination of complementary ultrasound markers in multiparametric ultrasound imaging. The further improvement in both the mean and the std values of AUC over the folds was observed when using MLSVD preprocessing, suggesting a more robust classification performance. The best performance was achieved by combining CUDI features with MLSVD preprocessing and SWE elasticity using a Gaussian kernel SVM classifier. Figure 2 shows an example of the histopathological SBx results and the PCa prediction results obtained by the proposed biopsy-region multiparametric ultra-sound imaging approach for the corresponding 12 regions in the same prostate. The biopsy regions with high prediction probability correspond to the regions with histopathologically confirmed csPCa.

IV. CONCLUSIONS

The proposed 3D multiparametric ultrasound imaging approach yields promising PCa classification results, especially by combination of tissue stiffness and vascularity-related ultrasound markers obtained with implemented dedicated DCE-US denoising step. These results reveal the diagnostic potential for cost-effective PCa localization by multiparametric ultrasound imaging.

In this work, we subdivided each 3D prostate into 12 regions according to the SBx template shown by Ukimura et al. [31]; however, the actual SBx locations may mismatch the template. Moreover, SBx may still miss cancer within the regions, resulting in underdiagnosis and overestimated number of false positives by multiparametric ultrasound. In the future, this limitation will be alleviated by correlating the parametric maps to the full-prostate pathology after radical prostatectomy; however, this requires accurate registration between 3D DCE-US, the reconstructed 3D SWE map, and the histopathological reference. In addition to the improved performance using all of the CUDI features, MLSVD improved the classification performance of each individual feature except for the system identification in [10]. This could be due to the eigenvalue regularization that was implemented to perform the inversion of the autocorrelation matrix. The information regarding the bubble movement might have been lost due to the additional

truncation. In this work, we focused on combining complementary ultrasound markers and the added benefit of using the MLSVD method by comparing the classification performances. Although five classifiers were used, the analysis of the difference in these classifiers was not included in this study. In the future, more statistical measures such as accuracy and F_1-score can be added to evaluate the classification performance for each classifier [32]. The k-fold cross-validation approach was employed in this work; however, the risk of over-fitting is high given the small number of patients. In the future, we will repeat the validation by dividing the 54 datasets into 9 folds with different combinations. Moreover, a multicenter trial has recently started to build a larger patient cohort, allowing further validation of the results and optimization of the classification performance.

Acknowledgment

References

[1] H. Sung, J. Ferlay *et al.*, "Global Cancer Statistics 2020: GLOBOCAN Estimates of Incidence and Mortality Worldwide for 36 Cancers in 185 Countries," *CA: A Cancer Journal for Clinicians*, vol. 71, no. 3, pp. 209–249, may 2021.

[2] A. Sidana, M. J. Watson *et al.*, "Fusion prostate biopsy outperforms 12-core systematic prostate biopsy in patients with prior negative systematic biopsy: A multi-institutional analysis," *Urologic oncology*, vol. 36, no. 7, pp. 341.e1–341.e7, jul 2018.

[3] F. Bladou, C. Fogaing *et al.*, "Transrectal ultrasound-guided biopsy for prostate cancer detection: Systematic and/or magnetic-resonance imaging-targeted," *Canadian Urological Association journal = Journal de l'Association des urologues du Canada*, vol. 11, no. 9, pp. E330–E337, sep 2017.

[4] J. O. Barentsz, J. Richenberg *et al.*, "ESUR prostate MR guidelines 2012," *Eur. Radiol.*, pp. 746–757, 2012.

[5] J. Folkman, "Role of angiogenesis in tumor growth and metastasis," *Seminars in oncology*, vol. 29, pp. 15–18, 2002.

[6] G. Russo, M. Mischi *et al.*, "Angiogenesis in prostate cancer: onset, progression and imaging," *BJU international*, vol. 110, pp. 749–808, dec 2012.

[7] M. P. Kuenen, M. Mischi *et al.*, "Contrast-ultrasound diffusion imaging for localization of prostate cancer," *IEEE Transactions on Medical Imaging*, vol. 30, no. 8, pp. 1493–1502, aug 2011.

[8] M. Mischi, M. P. Kuenen *et al.*, "Angiogenesis imaging by spatiotemporal analysis of ultrasound contrast agent dispersion kinetics," *IEEE Transactions on Ultrasonics, Ferroelectrics, and Frequency Control*, vol. 59, no. 4, pp. 621–629, apr 2012.

[9] S. G. Schalk, L. Demi *et al.*, "Contrast-Enhanced Ultrasound Angiogenesis Imaging by Mutual Information Analysis for Prostate Cancer Localization," *IEEE Transactions on Biomedical Engineering*, vol. 64, no. 3, pp. 661–670, mar 2017.

[10] R. J. van Sloun, L. Demi *et al.*, "Ultrasound-contrast-agent dispersion and velocity imaging for prostate cancer localization," *Medical Image Analysis*, vol. 35, pp. 610–619, jan 2017.

[11] R. R. Wildeboer, R. J. Van Sloun *et al.*, "Convective-Dispersion Modeling in 3D Contrast-Ultrasound Imaging for the Localization of Prostate Cancer," *IEEE Transactions on Medical Imaging*, vol. 37, no. 12, pp. 2593–2602, dec 2018.

[12] A. D. Bar-Zion, C. Tremblay-Darveau *et al.*, "Denoising of contrast-enhanced ultrasound cine sequences based on a multiplicative model," *IEEE Transactions on Biomedical Engineering*, vol. 62, no. 8, pp. 1969–1980, aug 2015.

[13] M. P. Kuenen, I. H. Herold *et al.*, "Maximum-likelihood estimation for indicator dilution analysis," *IEEE Transactions on Biomedical Engineering*, vol. 61, no. 3, pp. 821–831, mar 2014.

[14] R. R. Wildeboer, F. Sammali *et al.*, "Blind source separation for clutter and noise suppression in ultrasound imaging: Review for different applications," *IEEE Transactions on Ultrasonics, Ferroelectrics, and Frequency Control*, vol. 67, no. 8, pp. 1497–1512, 2020.

[15] M. Calis, A.-J. van der Veen *et al.*, "Denoising of Dynamic Contrast-enhanced Ultrasound Sequences: A Multilinear Approach," *Proceedings of the International Conference on Bio-inspired Systems and Signal Processing*, vol. 4, pp. 192–199, feb 2022.

[16] L. Pallwein, M. Mitterberger *et al.*, "Value of contrast-enhanced ultrasound and elastography in imaging of prostate cancer," *Current opinion in urology*, vol. 17, no. 1, pp. 39–47, jan 2007.

[17] J. M. Correas, A. M. Tissier *et al.*, "Prostate cancer: diagnostic performance of real-time shear-wave elastography," *Radiology*, vol. 275, no. 1, pp. 280–289, apr 2015.

[18] S. G. Schalk, A. Postema *et al.*, "3D surface-based registration of ultrasound and histology in prostate cancer imaging," *Computerized Medical Imaging and Graphics*, vol. 47, pp. 29–39, jan 2016.

[19] R. R. Wildeboer, R. J. van Sloun *et al.*, "3-D Multi-parametric Contrast-Enhanced Ultrasound for the Prediction of Prostate Cancer," *Ultrasound in Medicine and Biology*, vol. 45, no. 10, pp. 2713–2724, oct 2019.

[20] J. Tang, J. C. Yang *et al.*, "Enhancement characteristics of benign and malignant focal peripheral nodules in the peripheral zone of the prostate gland studied using contrast-enhanced transrectal ultrasound," *Clinical Radiology*, vol. 63, no. 10, pp. 1086–1091, oct 2008.

[21] N. Elie, A. Kaliski *et al.*, "Methodology for Quantifying Interactions Between Perfusion Evaluated by DCE-US and Hypoxia Throughout Tumor Growth," *Ultrasound in Medicine and Biology*, vol. 33, no. 4, pp. 549–560, apr 2007.

[22] A. W. Postema, P. J. Frinking *et al.*, "Dynamic contrast-enhanced ultrasound parametric imaging for the detection of prostate cancer," *BJU International*, vol. 117, no. 4, pp. 598–603, apr 2016.

[23] R. J. Eckersley, J. P. Michiel Sedelaar *et al.*, "Quantitative microbubble enhanced transrectal ultrasound as a tool for monitoring hormonal treatment of prostate carcinoma," *The Prostate*, vol. 51, no. 4, pp. 256–267, jun 2002.

[24] M. P. Kuenen, T. A. Saidov *et al.*, "Contrast-Ultrasound Dispersion Imaging for Prostate Cancer Localization by Improved Spatiotemporal Similarity Analysis," *Ultrasound in Medicine and Biology*, vol. 39, no. 9, pp. 1631–1641, sep 2013.

[25] M. P. Kuenen, T. A. Saidov *et al.*, "Spatiotemporal correlation of ultrasound contrast agent dilution curves for angiogenesis localization by dispersion imaging," *IEEE Transactions on Ultrasonics, Ferroelectrics, and Frequency Control*, vol. 60, no. 12, pp. 2665–2669, dec 2013.

[26] R. J. Van Sloun, L. Demi *et al.*, "Entropy of Ultrasound-Contrast-Agent Velocity Fields for Angiogenesis Imaging in Prostate Cancer," *IEEE Transactions on Medical Imaging*, vol. 36, no. 3, pp. 826–837, mar 2017.

[27] T. Saidov, C. Heneweer *et al.*, "Fractal Dimension of Tumor Microvasculature by DCE-US: Preliminary Study in Mice," *Ultrasound in medicine biology*, vol. 42, no. 12, pp. 2852–2863, dec 2016.

[28] R. J. Gillies, P. E. Kinahan *et al.*, "Radiomics: Images are more than pictures, they are data," *Radiology*, vol. 278, no. 2, pp. 563–577, feb 2016.

[29] P. Pudil, J. Novovičová *et al.*, "Floating search methods in feature selection," *Pattern Recognition Letters*, vol. 15, no. 11, pp. 1119–1125, nov 1994.

[30] T. Akiba, S. Sano *et al.*, "Optuna: A Next-generation Hyperparameter Optimization Framework," *Proceedings of the 25th ACM SIGKDD International Conference on Knowledge Discovery Data Mining*, 2019.

[31] O. Ukimura, J. A. Coleman *et al.*, "Contemporary role of systematic prostate biopsies: indications, techniques, and implications for patient care," *European urology*, vol. 63, no. 2, pp. 214–230, feb 2013.

[32] C. Goutte and E. Gaussier, "A probabilistic interpretation of precision, recall and f-score, with implication for evaluation," *Advances in Information Retrieval*, pp. 345–359, 2005.